JACS
JOURNAL OF THE AMERICAN CHEMICAL SOCIETY

Article

pubs.acs.org/JACS

Understanding THz and IR Signals beneath Time-Resolved Fluorescence from Excited-State Ab Initio Dynamics

Alessio Petrone,[†,§] Greta Donati,[†] Pasquale Caruso,[‡] and Nadia Rega*[,†,‡]

[†]Dipartimento di Scienze Chimiche, Università di Napoli 'Federico II', Complesso Universitario di M.S. Angelo, via Cintia, I-80126 Napoli, Italy

[‡]Italian Institute of Technology, IIT@CRIB Center for Advanced Biomaterials for Healthcare, Largo Barsanti e Matteucci, I-80125 Napoli, Italy

Supporting Information

ABSTRACT: The detailed interpretation of time-resolved spectroscopic signals in terms of the molecular rearrangement during a photoreaction or a photophysical event is one of the most important challenges of both experimental and theoretical chemistry. Here we simulate a time-resolved fluorescence spectrum of a dye in aqueous solution, the *N*-methyl-6-oxyquinolinium betaine, and analyze it in terms of far IR and THz frequency contributions, providing a direct connection to specific molecular motions. To obtain this result, we build up an innovative and general approach based on excited state ab-initio molecular dynamics and a wavelet-based time-dependent frequency analysis of nonstationary signals. We obtain a nice agreement with key parameters of the solvent dynamics, such as the total Stokes shift and the Stokes shift relaxation times. As an important finding, we observe a strong change of specific solute−solvent interactions upon the electronic excitation, with the migration of about 1.5 water molecules from the first solvation shell toward the bulk. In spite of this event, the Stokes shift dynamics is ruled by collective solvent motions in the THz and far IR, which guide and modulate the strong rearrangement of the dye microsolvation. By the relaxation of THz and IR contributions to the emission signal, we can follow and understand in detail the molecularity of the process. The protocol presented here is, in principle, transferable to other time-resolved spectroscopic techniques.

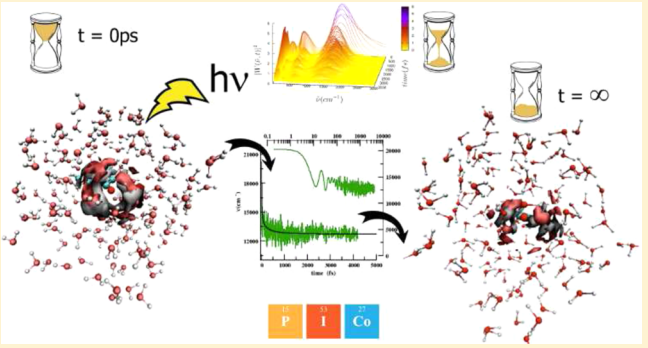

INTRODUCTION

Thanks to modern ultrafast pulsed laser techniques we are now able to observe far-from-equilibrium molecular structures that are literally *frozen* during a vibrational motion or a reaction and to monitor them on both the nuclear and the electronic time scales.[1−4]

In spite of this power, relating a spectroscopic signal to the detail of the atomistic dynamics is not a trivial task, especially when the nuclear motion is not detected by infrared or Raman probes but is instead recovered by the interpretation of optical absorption or emission signals. This is the case of time-resolved fluorescence, which can be considered the experimental technique of choice in many fields and is extensively adopted to investigate photoreactivity and solvent reorganization.[5−8] In studies of solvation dynamics, experimentally one usually monitors the time-dependent Stokes shift (TDSS), i.e., the time evolution of a solute emission peak. It is generally acknowledged that collective modes of the solvent dominate the relaxation process at short times,[9] and the TDSS can be modeled by continuum theories and/or by adopting ad hoc fitting procedures, without a direct molecular interpretation.[10−14]

Much less is known about the role played by a change of specific solute−solvent interactions, for example, when the number of solvation sites changes upon the solute electronic excitation.[11,15−17] An analysis of such a case at the molecular level would be important, to shed light on the capability of a dye to probe its environment. More in general, the comprehension of photophysics and photochemistry of probe-solvent specific interactions is a prototype of the influence of other interesting environments, like surfaces, DNA, proteins, or polymeric matrices.[18−20]

In this context the support from theory can be essential to enforce new models aimed at the analysis and the interpretation of experimental data. Indeed, providing a link between a spectroscopic signal and the atomistic reorganization of a far-from-equilibrium system is one of the main goals of modern theoretical chemistry.

Here we unveil and interpret THz and IR modes underlying the time-resolved fluorescence of a solvatochromic dye by means of an innovative theoretical approach.

Received: July 23, 2014
Published: September 22, 2014

dx.doi.org/10.1021/ja507518k | J. Am. Chem. Soc. 2014, 136, 14866−14874

The first ingredient of our strategy consists in the simulation of the time-resolved emission signal by means of excited state ab-initio molecular dynamics (AIMD). Methods to model the excited state dynamics are already well-known, either based on mean field approaches (Ehrenfest)[21,22] or by including population transfer between electronic states due to non-adiabatic events.[23−31] Moreover, the accuracy of AIMD,[21,32] based on energy and energy derivatives calculated by time-dependent density functional theory (TD-DFT),[33,34] has been already demonstrated.[35,36]

Once the time-resolved spectrum has been simulated, the relaxation function of the emission band peak can be calculated and decomposed in terms of a time-resolved frequency analysis. The latter is based on the wavelet theory that provides an unified framework for a number of techniques that have been developed independently for various applications on signal processing.[37−46] An analogue analysis can also be performed on the relaxation functions of some key structural parameters representing the reorganization underlying the spectroscopic time evolution. As result, THz and IR modes involved in the various relaxation processes monitored by time-resolved emission spectroscopy are unveiled and interpreted in the molecular detail.

As a challenging application, we analyzed the aqueous solvent relaxation following the $S_1 \leftarrow S_0$ excitation of a solvatochromic dye, the *N*-methyl-6-oxyquinolinium betaine (MQ, see Figure 1a). This system is very interesting because, as we find out and discuss in the following, a net change of specific interactions accompanies the solvation dynamics and the evolution of the Stokes shift. In particular, we observe a net loss of 1.4 water molecules from the first solvation shell triggered by the electronic excitation. The rearrangement of the first solvation shell therefore contributes to the large Stokes shift (about 7750 cm^{-1}). The several frequency contributions affecting the TDSS of the MQ molecule have been disentangled for the first time. We demonstrate that the change of specific interactions affects the Stokes shift dynamics only in the ultra fast part, while the rearrangement of the first solvation shell is ruled by collective solvent modes in the THz, mainly involving hydrogen bonds (HBs) networks. This also explains why well-established continuum theories of solvation dynamics still hold in this case.[47,48]

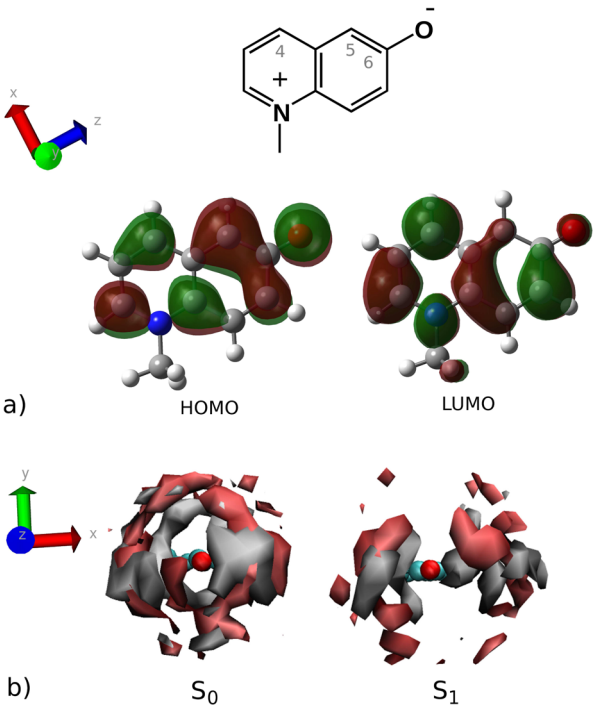

Figure 1. (a) *N*-methyl-6-oxyquinolinium betaine (MQ) structural formula and HOMO and LUMO contours calculated at the B3LYP/6-31(d,p) level of theory. (b) Spatial distribution functions of water oxygen (red) and hydrogen atoms (gray) belonging to the first solvation shell of the MQ oxygen. The view is directed onto the OC bond. Analysis refers to both the ground S_0 state (left) and the excited S_1 state (right) AIMD simulations.

The study presented here can be actually easily generalized as a protocol for understanding time-resolved spectroscopic signals and can find fruitful applications in many fields requiring a detailed knowledge of solute−solvent interaction dynamics, such as imaging techniques, biocatalysis, electrolyte-based dye-sensitized solar cells.

We present our method in the following section and then illustrate our findings in the Results Section, and give final remarks and perspectives as Conclusions.

METHODS

Simulation of the Stokes Shift Dynamics. From theory of time-dependent approaches to simulate spectroscopic signals, we learn that classical simulations at finite temperature can provide the necessary information to reproduce optical absorption/emission band shapes, although they are not capable, by nature, to account for the fine details of transition between vibronic states.[49] More closely, the spectroscopic line shape can be obtained by the following information: (1) a configurational distribution well-representative of the equilibrium in the initial electronic state of the chromophore under study and (2) corresponding values of the vertical electronic transition energy and dipole strength.

Therefore, properly simulating a chromophore in its environment (e.g., the solvent) at finite temperature in the ground state and then calculating excitation energies on a rightly chosen number of extracted frames gives us the way to simulate the steady state absorption spectrum.

Following this *classical mechanics* representation of spectroscopic events also for time-resolved signals, we can imagine the time-resolved emission spectrum accounted for by the instantaneous excitation of the ground state representative configurational distribution and by the subsequent evolution on the excited state potential energy surface toward the new equilibrium. The instantaneous spectroscopic line shape $L(\nu,t)$, a function of the frequency ν and time t, can be approximated as

$$L(\nu, t) = \int \rho(\mathbf{q}, t)|\mu_{eg}(\mathbf{q})|^2 \delta(V_e(\mathbf{q}) - V_g(\mathbf{q}) + h\nu)\mathrm{d}\mathbf{q} \quad (1)$$

where $\rho(\mathbf{q},t)$ is the configurational distribution of the coordinates $\mathbf{q}$ that is representative at time t, $|\mu_{eg}(\mathbf{q})|^2$ is the dipole strength of the electronic transition between the excited (e) and the ground (g) state, and $V_e(\mathbf{q}) - V_g(\mathbf{q})$ is vertical emission energy.

A mean value of $\nu(t)$, representative of the time-resolved emission peak, can be evaluated at each time step as

$$\nu(t) = \frac{\int L(\nu, t)\nu \mathrm{d}\nu}{\int L(\nu, t)\mathrm{d}\nu} \quad (2)$$

The $\nu(t)$ can be normalized with respect to the time necessary to conclude the relaxation process ($t = \infty$), obtaining

$$S(t) = (\nu(t) - \nu(\infty))/(\nu(0) - \nu(\infty)) \quad (3)$$

Thus, calculated emission energies and dipole strengths of a sample $\rho(\mathbf{q})$ evolving in the time after an electronic excitation bring us the

dx.doi.org/10.1021/ja507518k | J. Am. Chem. Soc. 2014, 136, 14866−14874

simulated TDSS, $S(t)$, that can be compared to the experimental counterpart.

It is worth noting that the *time zero* of the TDSS simulation corresponds to the steady-state absorption band mean value ($\nu(0)$), at variance of what happens experimentally, when the time zero depends upon the instrumental conditions.[50−52]

Time Domain Frequency Analysis. Beside the spectroscopic signal, excited state trajectories also account for the molecular relaxation accompanying the Stokes shift dynamics. Thus, both the TDSS and other relaxation functions of suitable structural parameters can be analyzed by a time-frequency decomposition, allowing us to disentangle in fine detail the IR and THz frequency contributions to the emission signal and to interpret them in terms of molecular influence on the chromophore.

Here we perform a multiresolution analysis by a continuous wavelet transform (WT), which is the appropriate one for our nonstationary time series.[37−40,53] The mathematical expression for the continuous WT simply replaces the Fourier basis function with a wavelet one:

$$W(a, b) = \int F(t)\psi_{a,b}(t)\mathrm{d}t \tag{4}$$

where $F(t)$ is a given relaxation function (for example, the simulated TDSS), and the wavelet function $\psi_{a,b}(t)$ is defined by dilation and translation of the mother wavelet $\psi(t)$, and it is modulated by the scale a, proportional to the inverse of frequency, and by the translation parameter b, representing the time localization:

$$\psi_{a,b}(t) = |a|^{-1/2}\psi\left(\frac{t-b}{a}\right)(a, b \in R;\ a \neq 0) \tag{5}$$

On the basis of preliminary tests, we chose the Morlet function as mother wavelet $\psi(t)$. By changing the wavelet scale and translation parameters, it is possible to analyze the spectrogram evolution during the time. In particular the frequency is localized in time by the b parameter, while the contributions of different frequencies are analyzed by varying the a value.

We obtain the wavelet power spectra by plotting $|W(\nu,t)|^2$, converting the scale factor in wavenumber. $|W(\nu,t)|^2$ is the time-dependent intensity of a frequency ν contributing to the $F(t)$ signal.[54] Thanks to this tool we are able to disentangle in the time domain the several frequencies tuning a relaxation function.

Simulation Details. The energy potential ruling the AIMD[55−61] performed in the present study was constructed according to the scheme described in refs 62−64. Briefly, the MQ molecule was treated by DFT and TD-DFT in the ground and the S_1 excited state, respectively, by adopting the global hybrid B3LYP[65] functional and the 6-31G(d,p) basis set. The barycenter of the MQ solute was fixed at the center of a sphere including about three shells of solvent molecules explicitly represented by the TIP3P[66] water model. Nonperiodic boundary conditions have been enforced,[62−64] accounting for interactions between the explicit molecular system and the implicit bulk solvent with both short-range dispersion−repulsion and long-range electrostatics interactions; the latter by including a polarizable continuum model.[67]

The scheme adopted here to define the potential energy surfaces has been extensively validated against experimental evidence in describing with high accuracy HBs structure and energetics, in both the ground and the excited electronic state.[63,64,68−71]

By adopting the same level of theory, we also performed a static analysis on isolated MQ (gas phase) and several representations of the MQ aqueous solution (full implicit, hybrid explicit/implicit for $MQ(H_2O)_n$ clusters, with n = 2, 4). This analysis was aimed to validate the mixed/classical potential in describing accurate MQ/solvent interactions and to disentangle several solvent effects (polarization, structural, specific interactions) on the total Stokes shift. This static approach required the calculation of vertical absorption and emission energy on minima obtained in the two electronic states for MQ in several environmental conditions. Harmonic frequencies were also evaluated, with numerical TD-DFT second energy derivatives adopted for calculations in the excited state.

We characterized the equilibrium of the ground (S_0) and the first singlet excited (S_1) states of MQ in aqueous solution, by performing equilibrium AIMD. From the sampling of the phase space in the ground state (AIMD trajectory in S_0) we chose 24 points as starting configurations and momenta of as many excited state MDs. The starting points were picked up to reproduce the main characteristics of the steady-state absorption band (average and the distribution of the electronic transition energies). Similarly, we ensured that the 24 points reproduce on average some key structural and dynamical features of the S_0 sample, such as the number of HBs to the MQ oxygen, and the total linear momentum.

Therefore, the MQ/water relaxation dynamics was reconstructed by collecting several (up to 24) AIMD trajectories on the S_1 potential energy surface, along with the corresponding evolution of the $S_1 \rightarrow S_0$ transition energy and dipole strength.

From these excited state trajectories we simulated the $S(t)$ signal according to the procedure sketched above. Moreover, three time-dependent structural parameters $f(t)$ were considered, whose $C(t)$ relaxation function has been calculated as

$$C(t) = \frac{\langle f(t)\rangle - \langle f(\infty)\rangle}{\langle f(0)\rangle - \langle f(\infty)\rangle} \tag{6}$$

where $\langle\cdots\rangle$ represents the average over the excited state trajectories at each time t. The three $f(t)$ parameters were chosen to follow in a thorough, simple, and dynamical way the evolution of the MQ first solvation shell and to characterize on the fly the molecular motion probed by the emission of the excited chromophore. Specifically, we chose the average number of water molecules within the first MQ solvation shell, $f_w(t)$, the average number of effective HBs involving the MQ oxygen $f_{HB}(t)$, and a function of the directional water H−O··· O MQ angle θ, $f_\theta(t)$, that represents the rearrangement of the water molecules orientation, calculated according to the expression defined in ref 72.

Wavelet power spectra of simulated spectroscopic and structural relaxation functions ($S(t)$, $C_{HB}(t)$, $C_w(t)$, and $C_\theta(t)$) allowed us to characterize how and when IR and THz modes of the solute and solvent molecules affect the Stokes shift dynamics of MQ in aqueous solution.

More details on methods discussed in this section, including results on the static energetic and structural analysis, are provided as Supporting Information (SI).

RESULTS

Microsolvation of MQ in S_0 and S_1 States. We first characterized the ground (S_0) and the first singlet excited (S_1) states of MQ in aqueous solution by analyzing the corresponding ab-initio trajectories.

The S_1 excited state does not show any significant multireference character and is obtained from S_0 by a HOMO → LUMO single excitation. As it can be observed from the frontier orbitals contours in Figure 1a, the $S_1 \leftarrow S_0$ transition is characterized by a substantial charge transfer from the MQ oxygen toward the quinolone ring and the nitrogen atom. From the microsolvation standpoint, the MQ−solvent interactions radically change upon excitation: in the ground state the oxygen site is able to engage specific solute−solvent interactions through the lone pair orbitals and the HOMO π lobe, while this latter is precluded in the S_1 state. In other words, the carbonyl group behaves as an anion in the ground state[68] and as a neutral group after the excitation. This also accounts for the reverse solvatochromism of MQ: the $S_1 \leftarrow S_0$ transition shifts to the blue when polarity is increased, since the HOMO is more stabilized by polar solvents compared to the LUMO. A blue shift of 0.67 eV was calculated when going from the gas phase (isolated molecule) to aqueous solution.

dx.doi.org/10.1021/ja507518k | J. Am. Chem. Soc. 2014, 136, 14866−14874

In Figure 1b we plot the isovalue surfaces of the spatial distribution functions for water oxygen (red) and hydrogen (gray) atoms, obtained from analysis of the AIMD performed in the two electronic states. These distributions cover the region around the MQ oxygen and summarize the most important features of MQ microsolvation. We observe a doughnut-shaped surface representing the water arrangement around the MQ oxygen in the ground state. Upon electronic excitation, the water spatial distribution reduces to two symmetrical lobes in the proximity of the oxygen lone pairs. This finding is mirrored by the radial distribution functions (RDFs) involving the MQ oxygen and the water molecules in the S_0 and the S_1 state at equilibrium, respectively, reported in Figure 2. We observe that the integration over the first peaks of

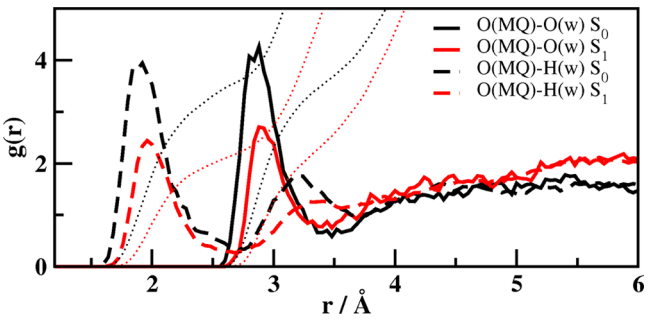

Figure 2. RDF's of MQ in aqueous solution, calculated by analysis of the AIMD trajectories in the ground (black) and the S_1 excited (red) state, respectively. The integration number of the distribution functions is also reported.

the oxygen−oxygen RDFs corresponds to 3.6 and 2.2 solvent molecules in the S_0 and S_1 case, respectively. From the analysis of the steady-state trajectories, the average number of HBs is 3.1 and 1.9 for the S_0 and the S_1, respectively. This implies a net loss of 1.4 water molecules in the MQ first solvation shell and of about one specific solute−solvent interaction, as consequence of the electronic excitation.

In a static picture, at the excited state the typical saturation of the MQ oxygen solvation sites (the two lone pairs) accounts for the microsolvation,[64,70,71] well-represented on average by a $MQ(H_2O)_2$ cluster, with two HBs in the main MQ molecular plane. Instead, at the ground state, a $MQ(H_2O)_4$ cluster is more representative, on average, of the MQ−solvent specific interactions. Indeed, previous X-ray diffraction and NMR experiments support our results in the electronic ground state.[73] In particular, the water spatial arrangement in the hydrated crystals suggests that the molecule is able to engage up to four HB interactions that are both colinear and orthogonal to the molecular plane.

The important rearrangement of the specific solute−solvent interactions (neat loss of 1.4 water molecules in the first solvation shell) also leads to a simulated Stokes shift of 7600 cm^{-1} (see below in the text), which nicely reproduces the experimentally observed value (around 7750 cm^{-1}). On the other hand, calculations of the Stokes shift performed on static MQ/water clusters indicated that, when considering the $MQ(H_2O)_2$ arrangement as representative of both the electronic states, the Stokes shift is strongly underestimated (see SI).

Stokes Shift Dynamics. The relaxation of the MQ/water system after the electronic excitation was followed for about 4 ps by 24 trajectories in the S_1 excited state. The corresponding time-resolved emission peak $\nu(t)$, calculated according to the procedure illustrated in the Methods section, is reported in Figure 3.

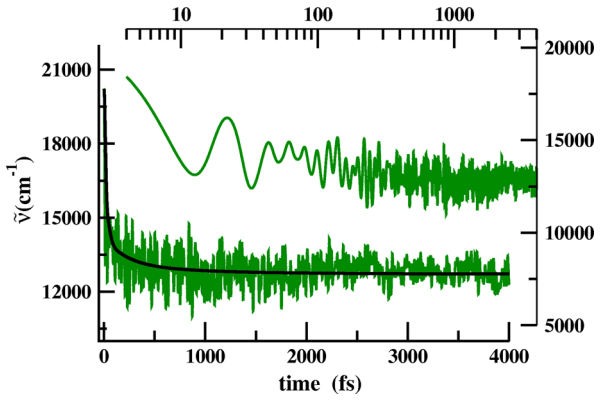

Figure 3. Time-dependent emission peak frequency (cm^{-1}, green) of MQ in aqueous solution, from nonequilibrium AIMD trajectories in the S_1 state. A representative curve (black) of stretched exponentials is also shown.

We observe an ultrafast decay of the $\nu(t)$ curve in about 50 fs, with a first recursive event at about 12 fs, followed by large oscillations. These correspond to a strong rearrangement of the quinolone ring, no sensible change in the first solvation shell being recorded during the first 50 fs (see below). This part of the ultrafast relaxation could not be detected experimentally due to limited instrumental resolution.[47]

Important features of the dynamics are in very good agreement with the experiment:[47] (1) the simulated full Stokes shift ($\nu(\infty) - \nu(0) \approx 7600$ cm^{-1}) agrees with the experimental difference between the absorption and stimulated emission maxima (≈7750 cm^{-1}); and (2) in spite of limited statistics, we also observe a decrease of the $\nu(t)$ oscillations after 2.5 ps when the experimental curve reaches a plateau, for an overall relaxation time (4 ps), that is also well-reproduced.

The normalized TDSS, $S(t)$, is compared to the experimental counterpart[47,74] in Figure 4.

At about 100 fs, the simulated $S(t)$ decay is slightly accelerated with respect to the experimental one. As tentative

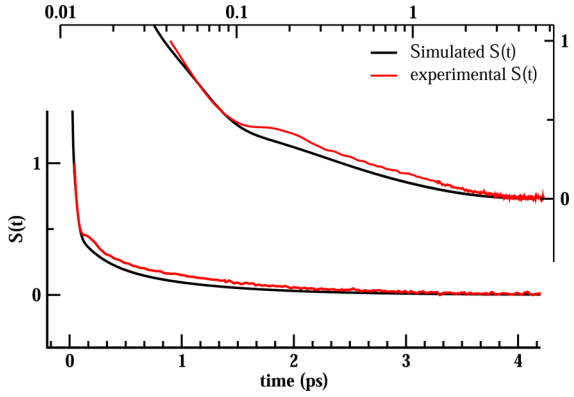

Figure 4. Normalized time-dependent Stokes shift of MQ in aqueous solution calculated from nonequilibrium AIMD trajectories in the S_1 state (black). Experimental curve (red, from ref 47) is shown for comparison. Simulated curve is shifted backward by the experimental resolution (35 fs).

dx.doi.org/10.1021/ja507518k | J. Am. Chem. Soc. 2014, 136, 14866−14874

explanation, we can probably attribute this behavior to the mixed quantum/classical energy potential, which may somehow favor a faster relaxation at early times.

However, the agreement between simulated and experimental $S(t)$ curves is overall good, also when disentangled in different relaxation times. As matter of fact, the analysis of experimental TDSS is usually carried out by fitting the curve with multiple exponential and Gaussian terms.[75] Here we performed a similar analysis: as reported in the SI, the decompositions of the simulated and experimental curves give comparable results. The simulated ultrafast contribution, not available experimentally, can be fitted by a Gaussian with a relaxation time τ of 19 fs.

Time-Resolved Frequency Analysis of TDSS. We analyzed the simulated TDSS, $S(t)$, in the time-frequency domains through the wavelet power spectrum, that is shown in Figure 5. The considered temporal range is 0−3200 fs, a time

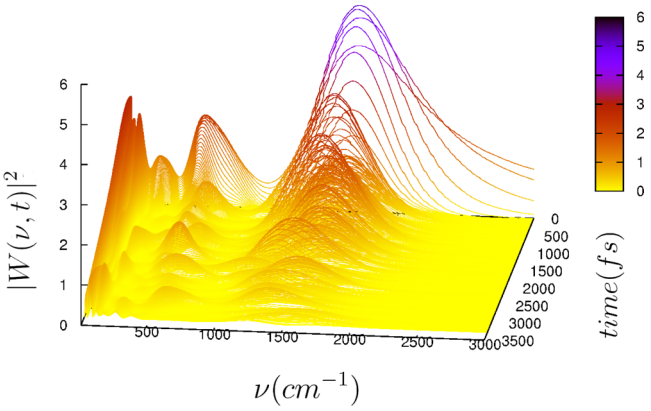

Figure 5. Wavelet power spectra of the simulated $S(t)$ for MQ in aqueous solution. Time and frequency are reported in fs and cm^{-1}, respectively. Wavelet power spectrum values $|W(\nu,t)|^2$ are expressed in arbitrary units.

sufficient for the $S(t)$ signal to reach a plateau and to almost complete the relaxation process. The plotted frequency range is 0−3000 cm^{-1}, because higher frequency values did not show any significant band. The most intense band at early times is centered around 1650 cm^{-1}. It can be easily assigned to the C═O stretching vibrational contribution to $S(t)$. This intramolecular contribution dominates the ultrafast relaxation, although it does not completely disappear in the time, becoming less relevant as long as the relaxation proceeds. This band also undergoes a pronounced red-shift during the process (about 80 cm^{-1}). Notably, this red-shift is in nice agreement with the results obtained by frequency calculations of representative MQ water clusters in the ground and the excited states (see Figure S3).

An intricate time evolution of several bands under 1000 cm^{-1} can be observed in the wavelet spectrum. It is reasonable to suppose that intramolecular MQ modes contribute to this range, at least in the ultrafast part. However, from frequency calculations performed on minima in the S_0 and S_1 states (see Figures S2 and S3), for both isolated MQ and MQ-water clusters, we observe that most important changes upon electronic excitation of MQ intramolecular modes regard the 1500−1750 cm^{-1} frequency range, while low-frequency modes are almost unaffected by the electronic excitation. Instead, solute−solvent intermolecular modes, such as the HB stretching modes, undergo not negligible changes. Therefore, we can reasonably assume that intramolecular MQ modes will not affect much the $S(t)$ power spectra below 1000 cm^{-1}, that are dominated by the solvent dynamics.

Far IR and THz frequencies of both bulk and hydration water have been the subject of many experimental and theoretical works.[76−80] It is recognized that contributions around 200 and 650 cm^{-1} are due to hindered longitudinal translations of water molecules in the HB network and to librational motions, respectively. Resonance around 80 cm^{-1} is attributed to HB bending motions. All these modes possess a collective character, involving up to two solvent shells around a single water molecule, as verified in detail by analysis of ab-initio simulations.[76]

In order to analyze the TDSS signal in terms of contributions due to the relaxation of different solvent modes, we defined frequency ranges in which the time-resolved bands can be approximately identified. Specifically, we chose the 400−800 cm^{-1} range, to follow a band peaked at about 590 cm^{-1} and attributed to the libration modes of water; the 150−400 cm^{-1} range, including recognizable bands assigned to collective HB stretching motions; the 75−150 cm^{-1} range, where bands are attributed to collective HB bending motions. Finally, we also monitored the 1000−2000 cm^{-1} range, to follow the C═O stretching relaxation.

For each frequency range we extracted the temporal evolution of the maximum intensity in the power spectrum, $|W(\nu,t)|^2_{max}$. These functions have been therefore fitted by exponential and Gaussian terms in order to analyze the corresponding relaxation times. Fitted curves are reported in Figure 6, while fitting parameters are given as SI.

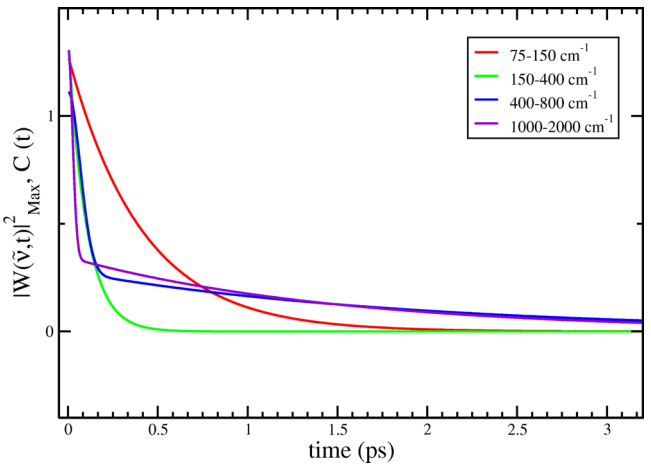

Figure 6. Fitted curves to maximum values of $S(t)$ wavelet spectrum, $|W(\nu,t)|^2_{max}$, calculated in different frequency ranges.

From inspection of Figure 6 we can see that the temporal evolution of the $|W(\nu,t)|^2_{max}$ amplitude is quite different in the several ranges. The band in the 1000−2000 cm^{-1} frequency range shows a stiff decay in the ultrafast part of the spectrum (relaxation time τ = 35 fs, see SI). Thus, the ultrafast part of the $S(t)$ decay, below the instrumental resolution, is dominated by the solute contribution represented by the C═O stretching. As already commented, the C═O band does not disappear, showing instead a residual relaxation (26%). This feature, however, cannot be considered an argument against the hypothesis of a Stokes shift mainly originated by the solvent reorganization. As matter of fact, the statistics of the sampling

dx.doi.org/10.1021/ja507518k | J. Am. Chem. Soc. 2014, 136, 14866−14874

in the excited state could be not sufficient to account for a very accurate relaxation of the C═O motions.

The dynamics of the band attributed to water librations (400−800 cm^{-1} range) is also characterized by an initial fast decay, followed by a slower evolution. Relaxation of the HB translational motions (150−400 cm^{-1} range) is initially similar to that of collective librations, although is completed in the fast part (250 fs). Collective HB bending motions (75−150 cm^{-1} range), on the other hand, relax in a slower way.

Relaxation times for THz and IR modes can be also compared with decay constants fitted to the experimental $S(t)$ curve. For example, relaxation of stretching and bending collective HB motions (τ = 101 and 410 fs, respectively) corresponds to a unique contribution fitted to the experimental curve with an average value of τ = 195 fs. On the other hand, collective water librations show a simulated relaxation time overestimated with respect to the experiment (τ = 95 vs 46 fs).

Molecularity of the Solvent Dynamics. We calculated the relaxation functions $C_{HB}(t)$, $C_w(t)$, and $C_\theta(t)$, describing the reorganization of the average number of HBs involving the MQ oxygen, the average number of water molecules belonging to the MQ oxygen first solvation shell, and the solvent molecules angular distribution in the first shell, respectively.

The solvation dynamics triggered by the MQ electronic excitation is first analyzed in the time-frequency domain, by the $C_\theta(t)$, $C_{HB}(t)$, and $C_w(t)$ wavelet power spectra shown in Figure 7 (upper, middle, and lower panels, respectively). The analyzed temporal range is the same used for the TDSS power spectrum, i.e., 0−3200 fs. On the other hand, the frequency range is 0−1000 cm^{-1}, because higher frequency values did not show any significant contribution. That means, the dynamics of the MQ microsolvation is not affected by the C═O stretching relaxation and only depends upon the collective solvent motions below 1000 cm^{-1}.

It is evident that a rich region below 250 cm^{-1} is present in all the spectra, proving that the microsolvation relaxation is strongly influenced by the collective HB stretching and bending motions. By an inspection of $C_\theta(t)$ and $C_{HB}(t)$ wavelet spectra, we can see a more important contribution of bands arising from collective water librational motions (400−800 cm^{-1} range), especially in the first case, representing the relaxation of water molecules spatial orientation. In the $C_w(t)$ spectrum, on the other hand, this contribution is less important.

At this point it is useful to compare the $C(t)$'s with the TDSS, as done in Figure 8. Notably, the TDSS and the overall solvent structural relaxation, including the change of specific interactions, show a similar progress in time. This means that the change of specific interactions between the chromophore and solvent molecules ($C_{HB}(t)$), the rearrangement of the water orientation ($C_\theta(t)$), and the migration of molecules from the solute toward the bulk ($C_w(t)$) are ruled by the same decay processes beneath the $S(t)$ signal, i.e., by the collective solvent rearrangement. More in detail, in Figure 9 we observe that the relaxation of the HB number around the MQ oxygen, given by $C_{HB}(t)$, retraces the collective HB stretching and bending contributions to $S(t)$, represented by the $|W(\nu,t)|^2_{max}$ functions in the 75−150 and 150−400 cm^{-1} ranges. An analogue comparison is reported in Figure 10, where the relaxation of the water orientation, given by $C_\theta(t)$, can be mainly related to the librational contribution to the TDSS ($|W(\nu,t)|^2_{max}$ in the 400−800 cm^{-1} range).

We are now able to understand the molecularity of the Stokes shift dynamics. Upon the MQ excitation, an

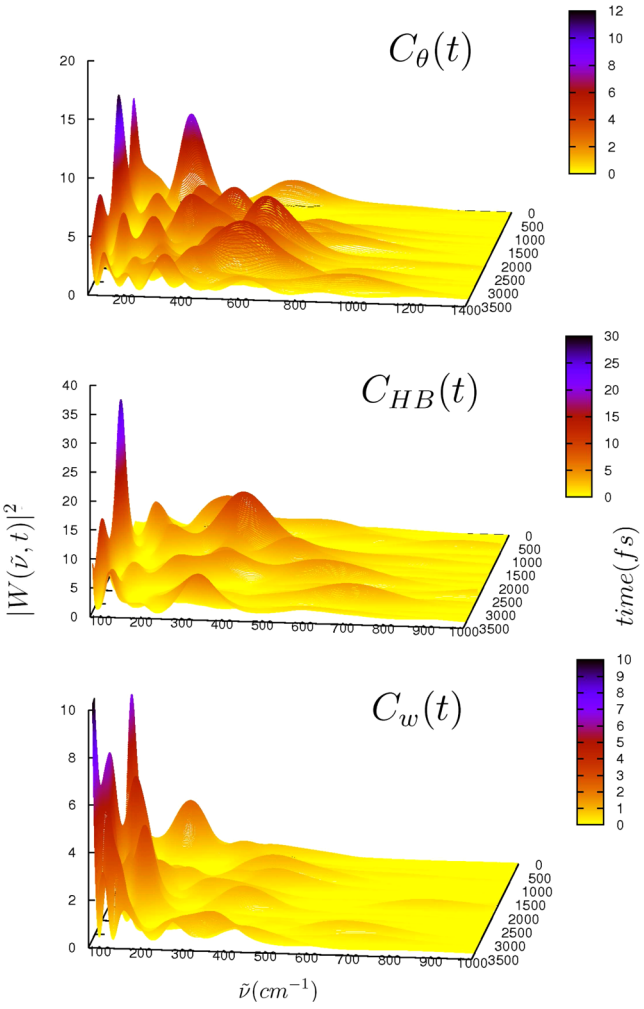

Figure 7. Wavelet power spectra of the $C_\theta(t)$ (upper panel), $C_{HB}(t)$ (middle panel), and $C_w(t)$ (lower panel) structural relaxation functions for MQ in aqueous solution. Time and frequency are reported in fs and cm^{-1}, respectively. Wavelet power spectrum values $|W(\nu,t)|^2$ are expressed in arbitrary units.

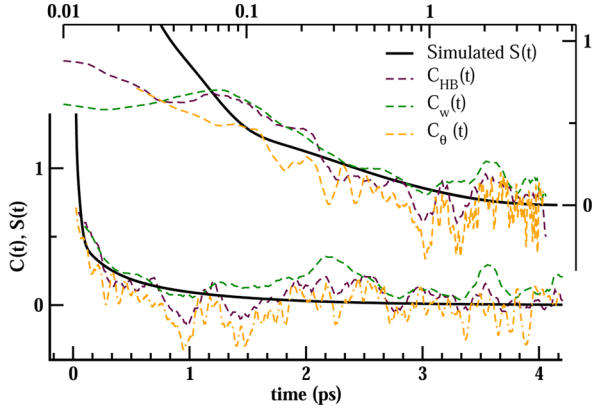

Figure 8. Averaged values of relaxation functions of MQ solvation dynamics obtained by the analysis of nonequilibrium AIMD trajectories in the S_1 state: number of waters within the first solvation shell, $C_w(t)$ (broken green line), number of MQ/water HBs, $C_{HB}(t)$ (broken maroon line), and water orientational relaxation function, $C_\theta(t)$ (broken orange line). The simulated representative curve of MQ TDSS, $S(t)$, is also reported for comparison (black full line).

dx.doi.org/10.1021/ja507518k | J. Am. Chem. Soc. 2014, 136, 14866−14874

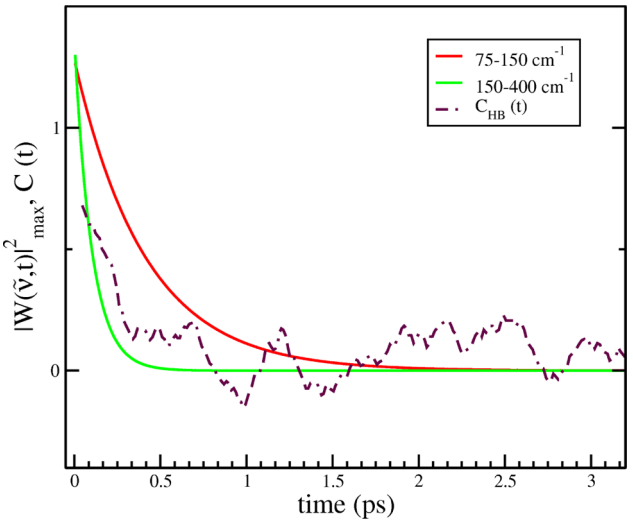

Figure 9. Maximum values of $S(t)$ wavelet spectra, $|W(\nu,t)|^2_{max}$, compared to the number of MQ/water HBs, $C_{HB}(t)$, of MQ solvation dynamics.

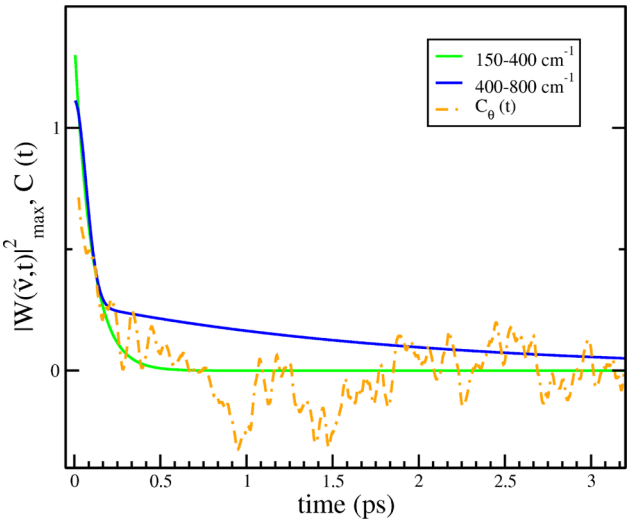

Figure 10. Maximum values of $S(t)$ wavelet spectra, $|W(\nu,t)|^2_{max}$, compared to the water molecules orientation relaxation function, $C_\theta(t)$, of MQ solvation dynamics.

instantaneous loss of solute−solvent interactions, previously involving the π density on the MQ oxygen, takes place. This event accounts for a significant part of the entire Stokes shift. During this time, however, the water molecules of the first shell remain in the solute proximity. Then, collective water motions drive the change of the first shell composition. From the analysis of the TDSS in different frequency ranges, we can deduce that, during the first 250 fs, collective water librations and HB stretching motions drive the change of HBs to the MQ oxygen with a fast rearrangement. In the first 2 ps, the molecules reorganize mainly through collective HB bending motions (15−150 cm^{-1}). At longer times (after ∼2 ps), the low-frequency (<75 cm^{-1}) modes dominate the relaxation.[81] This is approximately the time when both the experimental and the simulated $S(t)$ curves reach a plateau, i.e., the overall relaxation process is almost completed.

As important finding in this work, the change in the number of specific solute−solvent interactions has an important consequence on the total amount of the Stokes shift but not on its dynamics. The migration of solvent molecules toward external shells appears similar to a diffusion phenomenon in the bulk, mainly ruled by the rearrangement of collective solvent motions, rather than by solute−solvent coupling, operating on a faster time scale. In other words, the specific event triggered by the solute electronic excitation, namely the change in the composition of the first solvation shell, is modulated by the fluctuations of the bulk solvent. This also explains why models based on continuum theories nicely reproduce the MQ solvation dynamics.[47]

CONCLUSIONS

By means of time-dependent frequency analysis of excited-state AIMD trajectories, we simulated the time-dependent Stokes shift of the MQ solvatochromic dye and disentangled it in terms of IR and THz frequency contributions to the solvent reorganization. We validated our method by finding a nice agreement with the experiment for what regards photophysical key features, such as the total Stokes shift amount and the Stokes shift relaxation times.

Although the MQ dye undergoes a neat change of solute−solvent specific interactions (decrease of HB average number) upon the electronic excitation, our results clearly show that the Stokes shift dynamics is ruled by collective solvent motions, which drive the migration of 1.4 water molecules from the first into the second shell of solvation in about 4 ps. This finding explains how the TDSS can be nicely described by continuum theories, even if an important change of specific solute−solvent interactions are involved.

The main advantage of the method presented here is the capability to unveil molecularity of processes beneath complex time-resolved spectroscopic signals, providing a direct interpretation of the photochemical or photophysical event under study. More in general, this kind of study can also shed light on other fundamental mechanisms by which a solute passes a given *information* to the aqueous solvent, as it happens for the transmission of magnetic properties in imaging techniques, where the measured relaxation times are frequently used to produce contrast in magnetic resonance images,[82] or when a product of a reaction involving the solute and a solvent molecule migrates in the bulk, as it happens often in biocatalysis or in the new electrolyte-based dye-sensitized solar cells, in which it is crucial to enhance the charge transport ability and the efficiency.[83] Our current work addresses these important issues.

ASSOCIATED CONTENT

Supporting Information

Computational and methodological details regarding the hybrid explicit/implicit solvation scheme, the static analysis on $MQ(H_2O)_n$ (n = 2,4) clusters, the ab-initio dynamics at equilibrium in the ground and the excited states, the starting configurations to obtain the Stokes shift dynamics, the definition of structural relaxation functions, the wavelet analysis, the multiexponential fit of relaxation curves and all the structures optimized in the present study. This material is available free of charge via the Internet at http://pubs.acs.org.

AUTHOR INFORMATION

Corresponding Author

nadia.rega@unina.it

Present Address
[§]Department of Chemistry, University of Washington, Seattle, Washington, USA.

Notes
The authors declare no competing financial interest.

■ ACKNOWLEDGMENTS

N.R. and A.P. are grateful to Prof. N. Ernsting (Humboldt University, Berlin) for useful discussions and suggestions and for reading an early version of the manuscript. All the authors thank Gaussian Inc. for financial support.

■ REFERENCES

(1) Zewail, A. H. *Angew. Chem., Int. Ed.* **2000**, *39*, 2586−2631.
(2) Frontiera, R. R.; Mathies, R. A. *Laser Photonics Rev.* **2011**, *5*, 102−113.
(3) Fang, C.; Frontiera, R. R.; Tran, R.; Mathies, R. A. *Nature* **2009**, *462*, 200−204.
(4) Rini, M.; Magnes, B. Z.; Pines, E.; Nibbering, E. T. *Science* **2003**, *301*, 349−352.
(5) Reid, G. D.; Wynne, K. *Handbook of Laser Technology and Applications. Vol. III: Applications*; IOP Publishing Ltd: Philadelphia, PA, 2004; Vol. *III*: Applications, p 2003.
(6) Kondo, M.; Heisler, I. A.; Stoner-Ma, D.; Tonge, P. J.; Meech, S. R. *J. Am. Chem. Soc.* **2009**, *132*, 1452−1453.
(7) Rolczynski, B. S.; Szarko, J. M.; Son, H. J.; Liang, Y.; Yu, L.; Chen, L. X. *J. Am. Chem. Soc.* **2012**, *134*, 4142−4152.
(8) Quick, M.; Weigel, A.; Ernsting, N. P. *J. Phys. Chem. B* **2013**, *117*, 5441−5447.
(9) Nandi, N.; Roy, S.; Bagchi, B. *J. Chem. Phys.* **1995**, *102*, 1390−1397.
(10) Jimenez, T. R.; Fleming, G. R.; Kumar, V.; Maroncelli, M. *Nature* **1994**, *369*, 471−473.
(11) Chapman, C. F.; Fee, R. S.; Maroncelli, M. *J. Phys. Chem.* **1995**, *99*, 4811−4819.
(12) Song, X.; Chandler, D. *J. Chem. Phys.* **1998**, *108*, 2594−2600.
(13) Georgievskii, Y.; Hsu, C.-P.; Marcus, R. A. *J. Chem. Phys.* **1998**, *108*, 7356−7366.
(14) Bagchi, B. *J. Chem. Phys.* **1994**, *100*, 6658−6664.
(15) Sajadi, M.; Obernhuber, T.; Kovalenko, S. A.; Mosquera, M.; Dick, B.; Ernsting, N. P. *J. Phys. Chem. A* **2009**, *113*, 44−55.
(16) Yu, J.; Berg, M. *Chem. Phys. Lett.* **1993**, *208*, 315−320.
(17) Benigno, A. J.; Ahmed, E.; Berg, M. *J. Chem. Phys.* **1996**, *104*, 7382−7394.
(18) Furse, K. E.; Corcelli, S. A. *J. Phys. Chem. Lett.* **2010**, *100*, 1813−1820.
(19) Nandi, N.; Bhattacharyya, K.; Bagchi, B. *Chem. Rev.* **2000**, *100*, 2013−2045.
(20) Bagchi, B. *Annu. Rev. Phys. Chem.* **1996**, *47*, 109−134.
(21) Bolton, K.; Hase, W. L.; Peslherbe, G. H. *Modern Methods for Multidimensional Dynamics Computation in Chemistry*; D. L. Thompson, Ed.; World Scientific: Singapore, 1998; Vol. *95*; pp 143−189.
(22) Li, X.; Tully, J. C.; Schlegel, H. B.; Frisch, M. J. *J. Chem. Phys.* **2005**, *123*, 084106.
(23) Tully, J. C. *J. Chem. Phys.* **1990**, *93*, 1061−1071.
(24) Martinez, T.; Ben-Nun, M.; Levine, R. *J. Phys. Chem.* **1996**, *100*, 7884−7895.
(25) Martinez, T. J. *Acc. Chem. Res.* **2006**, *39*, 119−126.
(26) Tapavicza, E.; Tavernelli, I.; Rothlisberger, U. *Phys. Rev. Lett.* **2007**, *98*, 023001.
(27) Thompson, A. L.; Martinez, T. J. *Faraday Discuss.* **2011**, *150*, 293−311.
(28) Tapavicza, E.; Bellchambers, G. D.; Vincent, J. C.; Furche, F. *Phys. Chem. Chem. Phys.* **2013**, *15*, 18336−18348.
(29) Spoerkel, L.; Cui, G.; Koslowski, A.; Thiel, W. *J. Phys. Chem. A* **2014**, *118*, 152−157.
(30) Nelson, T.; Prezhdo, O. *J. Am. Chem. Soc.* **2013**, *135*, 3702−3710.
(31) Wohlgemuth, M.; Bonai-Koutecky, V.; Mitri, R. *J. Chem. Phys.* **2011**, *135*, 054105−054109.
(32) Millam, J. M.; Bakken, V.; Chen, W.; Hase, W. L.; Schlegel, H. B. *J. Chem. Phys.* **1999**, *111*, 3800−3805.
(33) Gross, E. K. U.; Kohn, W. *Phys. Rev. Lett.* **1985**, *55*, 2850−2852.
(34) Stratmann, R. E.; Scuseria, G. E.; Frisch, M. J. *J. Chem. Phys.* **1998**, *109*, 8218−8224.
(35) Tavernelli, I.; Röhrig, U. F.; Rothlisberger, U. *Mol. Phys.* **2005**, *103*, 963−981.
(36) Guglielmi, M.; Tavernelli, I.; Rothlisberger, U. *Phys. Chem. Chem. Phys.* **2009**, *11*, 4549−4555.
(37) Walnut, D. F. *An introduction to Wavelet Analysis*; Birkhäuser Boston, c/o Springer-Verlag: New York, 2002.
(38) Rioul, O.; Vetterli, M. *IEEE Signal Process. Mag.* **1991**, *8*, 14−38.
(39) Daubechies, I. *IEEE Trans. Inf. Theory* **1990**, *36*, 961−1005.
(40) Torrence, C.; Compo, C. P. *Bull. Am. Meteorol. Soc.* **1998**, *79*, 61−78.
(41) Otsuka, T.; Nakai, H. *J. Comput. Chem.* **2007**, *28*, 1137−1144.
(42) Pagliai, M.; Muniz-Miranda, F.; Cardini, G.; Righini, R.; Schettino, V. *J. Phys. Chem. Lett.* **2010**, *1*, 2951.
(43) Mallik, B. S.; Chandra, A. *J. Mol. Liq.* **2008**, *143*, 31.
(44) Pagliai, M.; Muniz-Miranda, F.; Cardini, G.; Righini, R.; Schettino, V. *J. Mol. Struct.* **2011**, *993*, 438−442.
(45) Dietrick, S. M.; Pacheco, A. B.; Phatak, P.; Stevens, P. S.; Iyengar, S. S. *J. Phys. Chem. A* **2012**, *116*, 399−414.
(46) Prociuk, A. H.; Iyengar, S. S. *J. Chem. Theory Comput.* **2014**, *10*, 2950−2963.
(47) Pérez-Lustres, J.; Kovalenko, S.; Mosquera, M.; Senyushkina, T.; Flasche, W.; Ernsting, N. *Angew. Chem., Int. Ed.* **2005**, *44*, 5635−5639.
(48) Sajadi, M.; Ajaj, Y.; Loffe, I.; Weingartner, H.; Ernsting, N. P. *Angew. Chem., Int. Ed.* **2010**, *49*, 454−457.
(49) Barone, V. *Computational strategies for spectroscopy: from small molecules to nano systems*; John Wiley and Sons: Hoboken, NJ, 2011; pp 503−514.
(50) Maroncelli, M.; Fleming, G. R. *J. Chem. Phys.* **1988**, *89*, 875−881.
(51) Maroncelli, M. *J. Mol. Liq.* **1993**, *57*, 1−37.
(52) Kumar, P. V.; Maroncelli, M. *J. Chem. Phys.* **1995**, *103*, 3038−3060.
(53) Carmona, R.; Hwang, W.-L.; Torrésani, B. *Practical Time-Frequency Analysis: Gabor and Wavelet Transforms, with an Implementation in S*; Academic Press: San Diego, CA, 1998; Vol. *9*.
(54) Note that the magnitude of the wavelet power spectra is not the quantum electric dipole cross-section in terms of normal modes, rather it is the time-resolved, out of equilibrium version of the standard spectroscopical analysis from classical MD simulation. As such, we observe classical and intrisically anharmonic modes activated at a finite temperature according to the equipartition of the kinetic energy.
(55) Schlegel, H. B.; Millam, J. M.; Iyengar, S. S.; Voth, G. A.; Daniels, A. D.; Scuseria, G. E.; Frisch, M. J. *J. Chem. Phys.* **2001**, *114*, 9758−9763.
(56) Iyengar, S. S.; Schlegel, H. B.; Millam, J. M.; Voth, G. A.; Scuseria, G. E.; Frisch, M. J. *J. Chem. Phys.* **2001**, *115*, 10291−10302.
(57) Schlegel, H. B.; Iyengar, S. S.; Li, X.; Millam, J. M.; Voth, G. A.; Scuseria, G. E.; Frisch, M. J. *J. Chem. Phys.* **2002**, *117*, 8694−8704.
(58) Bunker, D. L. *Meth. Comp. Phys.* **1971**, *10*, 287−325.
(59) Raff, L. M.; Thompson, D. L. *Theory of Chemical Reaction Dynamics*; CRC: Boca Raton, FL, 1985.
(60) *Advances in Classical Trajectory Methods*; Hase, E. W. L., Ed.; JAI: Stamford, CT, 1991.
(61) Helgaker, T.; Uggerud, E.; Jensen, H. J. A. *Chem. Phys. Lett.* **1990**, *173*, 145−150.
(62) Rega, N.; Brancato, G.; Barone, V. *Chem. Phys. Lett.* **2006**, *422*, 367−371.
(63) Brancato, G.; Barone, V.; Rega, N. *Theor. Chem. Acc.* **2007**, *117*, 1001−1015.

(64) Brancato, G.; Rega, N.; Barone, V. *J. Chem. Phys.* **2008**, *128*, 144501−10.
(65) Becke, A. D. *J. Chem. Phys.* **1993**, *98*, 5648−5652.
(66) Jorgensen, W. L.; Chandrasekhar, J.; Madura, J. D.; Impey, R. W.; Klein, M. L. *J. Chem. Phys.* **1983**, *79*, 926−935.
(67) Cossi, M.; Rega, N.; Scalmani, G.; Barone, V. *J. Comput. Chem.* **2003**, *24*, 669−681.
(68) Brancato, G.; Rega, N.; Barone, V. *J. Am. Chem. Soc.* **2007**, *129*, 15380−15390.
(69) Rega, N.; Brancato, G.; Petrone, A.; Caruso, P.; Barone, V. *J. Chem. Phys.* **2011**, *134*, 074504.
(70) Brancato, G.; Rega, N.; Barone, V. *J. Chem. Phys.* **2006**, *125*, 164515−11.
(71) Brancato, G.; Rega, N.; Barone, V. *Chem. Phys. Lett.* **2008**, *453*, 202−206.
(72) Pagliai, M.; Cardini, G.; Righini, R.; Schettino, V. *J. Chem. Phys.* **2003**, *119*, 6655−6662.
(73) Barczyński, P.; Ratajczak-Sitarz, M.; Katrusiak, A.; Szafran, M. *J. Mol. Struct.* **2010**, *976*, 87−96.
(74) Sajadi, M.; Weinberger, M.; Wagenknecht, H.; Ernsting, N. *Phys. Chem. Chem. Phys.* **2011**, *13*, 17768−17774.
(75) Hsu, C.; Song, X.; Marcus, R. *J. Phys. Chem. B* **1997**, *101*, 2546−2551.
(76) Heyden, M.; Sun, J.; Funkner, S.; Mathias, G.; Forbert, H.; Havenith, M.; Marx, D. *Proc. Natl. Acad. Sci. U.S.A.* **2010**, *107*, 12068−12073.
(77) Zelsmann, H. *J. Mol. Struct.* **1995**, *350*, 95−114.
(78) Bertie, J.; Lan, Z. *Appl. Spectrosc.* **1996**, *50*, 1047−1057.
(79) Walrafen, G. *J. Chem. Phys.* **1990**, *94*, 2237−2239.
(80) Ohmine, I.; Saito, S. *Acc. Chem. Res.* **1999**, *32*, 741−749.
(81) Ellison, W. *J. Phys. Chem. Ref. Data* **2007**, *36*, 1−18.
(82) Britton, M. M. *Chem. Soc. Rev.* **2010**, *39*, 4036−4043.
(83) ORegan, B. C.; Durrant, J. R. *Acc. Chem. Res.* **2009**, *42*, 1799−1808.